Inorganic Chemistry
Article

Inorg. Chem. **2010**, *49*, 1651–1657 **1651**
DOI: 10.1021/ic902053b

Unprecedented Layered Inorganic−Organic Hybrid Compound $Mn_3Sb_2S_6(C_6H_{18}N_4)$ Composed of $Mn_4Sb_2S_6$ Double-Cubane Units Showing Magnetic Long-Range Order and Frustration

Zomaje Rejai,[†] Henning Lühmann,[†] Christian Näther,[†] Reinhard K. Kremer,[‡] and Wolfgang Bensch*[,†]

[†]*Institut für Anorganische Chemie, Christian-Albrechts-Universität zu Kiel, Max-Eyth-Strasse 2, D-24118 Kiel, Germany and* [‡]*Max-Planck Institut für Festkörperforschung, Heisenbergstrasse 1, D-70506 Stuttgart, Germany*

Received October 16, 2009

The title compound $Mn_3Sb_2S_6(C_6H_{18}N_4)$ ($C_6H_{18}N_4$ = triethylenetetramine) was obtained under solvothermal conditions by reacting Mn, Sb, S, and the amine at 140 °C for 7 days. The compound crystallizes in the triclinic space group $P\bar{1}$ with a = 6.645(1) Å, b = 8.667(1) Å, c = 9.660(1) Å, α = 90.82(2)°, β = 109.70(2)°, γ = 110.68(2)°, Z = 1, and V = 484.4(1) Å^3. The $Mn_4Sb_2S_6$ double-heterocubane unit is the main motif in the structure of the title compound, which results from the interconnection of two SbS_3 trigonal pyramids, two MnS_6 octahedra, and two MnS_4N_2 octahedra. The two N atoms completing the environment of the latter Mn^{2+} ions belong to the tetradentate amine; i.e., the amine acts in a bidentate manner. The $Mn_4Sb_2S_6$ groups are joined by corner sharing of the MnS_6 octahedra, yielding one-dimensional linear $Mn_3Sb_2S_6$ rods along [100]. The two other N atoms of the amine molecule act in a bidentate manner to Mn^{2+} ions of neighboring rods, thus producing layers within the (010) plane. Within the rods, the arrangement of the Mn^{2+} ions in triangles leads to a chain of Mn^{2+} diamonds connected via opposite corners. For the magnetic properties, each edge connecting the Mn^{2+} ions represents a superexchange path due to coupling of the Mn^{2+} centers via S bridges. The resulting Mn^{2+} triangles give rise to substantial competing interaction and magnetic frustration. Below about 100 K, a gradual buildup of short-range antiferromagnetic correlations is observed. At lower temperatures, long-range antiferromagnetic interactions occur with T_N = 2.90 K, as indicated by a λ-type anomaly in the heat capacity curve. The analysis of the magnetic and heat capacity data evidences that the magnetic properties are essentially determined by the one-dimensional character of the $Mn_3Sb_2S_6$ chain. In addition, significant magnetic frustration due to the arrangement of the Mn^{2+} ions in a triangular configuration cannot be neglected.

Introduction

Transition-metal-containing thioantimonate(III) compounds are obtained under solvothermal conditions by applying suitable amines as structure-directing molecules. Many transition metals form stable coordinatively saturated complexes with the amines, and therefore these complexes cannot form bonds to the inorganic network but rather act as space fillers and charge-compensating molecules. A few years ago we presented a new strategy to incorporate transition metals into thioantimonate(III) networks.[1,2] According to this synthetic approach, a multidentate amine is required, which saturates only four of the possible coordination sites at the transition-metal ion, allowing one or two binding sites to be free for bond formation to the inorganic network. The feasibility of this idea was demonstrated using Mn, Fe, Co, Ni, or Zn as transition metals.[1−8] However, an analysis of the known thioantimonate(III) compounds containing Mn^{2+} ions evidences that such a strategy is not necessarily a prerequisite for bond formation to S atoms of the thioantimonate(III) network. The first examples of charge-neutral Mn^{2+}-containing thioantimonate(III) networks were the $Mn_2(A)Sb_2Sb_5$ compounds synthesized from amines A = ethylamine, methylamine, diethylenetriamine, ethylenediamine, 1,3-diaminopropane, *N*-methyl-1,3-diaminopropane, and diaminopentane.[9−14] In this family of compounds, SbS_3

*To whom correspondence should be addressed. E-mail: wbensch@ac.uni-kiel.de. Fax: +49-(0)431-880-1520.

(1) Stähler, R.; Bensch, W. *J. Chem. Soc., Dalton Trans.* **2001**, 2518.
(2) Stähler, R.; Bensch, W. *Eur. J. Inorg. Chem.* **2001**, 3073.
(3) Kiebach, R.; Bensch, W.; Hoffmann, R.-D.; Pöttgen, R. *Z. Anorg. Allg. Chem.* **2003**, *629*, 532.
(4) Schaefer, M.; Näther, C.; Bensch, W. *Solid State Sci.* **2003**, *5*, 1135.
(5) Schaefer, M.; Stähler, R.; Kiebach, W.-R.; Näther, C.; Bensch, W. *Z. Anorg. Allg. Chem.* **2004**, *630*, 1816.
(6) Schaefer, M.; Näther, C.; Bensch, W. *Monatsh. Chem.* **2004**, *135*, 461.
(7) Schaefer, M.; Näther, C.; Lehnert, N.; Bensch, W. *Inorg. Chem.* **2004**, *43*, 2914.
(8) Schaefer, M.; Kurowski, D.; Pfitzner, A.; Näther, C.; Rejai, Z.; Möller, K.; Ziegler, N.; Bensch, W. *Inorg. Chem.* **2006**, *45*, 3726.
(9) Bensch, W.; Schur, M. *Eur. J. Solid State Inorg. Chem.* **1996**, *33*, 1149.
(10) Bensch, W.; Schur, M. *Z. Naturforsch.* **1997**, *52b*, 405.
(11) Schur, M.; Näther, C.; Bensch, W. *Z. Naturforsch.* **2001**, *56b*, 79.
(12) Schur, M.; Bensch, W. *Z. Naturforsch.* **2002**, *57b*, 1.
(13) Engelke, L.; Stähler, R.; Schur, M.; Näther, C.; Bensch, W.; Pöttgen, R.; Möller, M. H. *Z. Naturforsch.* **2004**, *59b*, 869.

Published on Web 01/12/2010

trigonal pyramids and MnS_6 and MnS_4N_2 octahedra are joined to form strong distorted heterocubane groups. These heterocubanes share common corners and edges, yielding the layered $Mn_2(A)Sb_2S_5$ structure. The connection pattern leaves ellipsoidal holes within the layers. The charge-neutral layers are stacked in a manner in which the amines fill the interlayer space and also partially the holes. The magnetic properties of the compounds are typical for frustrated magnetic systems; i.e., despite the very large negative values for the Weiss constant, no long-range order is observed down to 4 K.[13] A remarkable structural feature is a very long Mn−S bond ranging from about 2.8 to 3.2 Å depending on the amine in the structure.[13] In natural minerals, several Mn^{2+}-containing thioantimonate(III) compounds were identified as sulfides (sulfosalts) with complex compositions. Examples are $AgPb_3MnSb_5S_{12}$ (uchuchacuaite),[20,21] $MnPb_4Sb_6S_{14}$ (benavidesite),[22] $Ag_4MnSb_2S_6$ (samsonite),[23] or the simpler compound $MnSb_2S_4$ (clerite and the monoclinic polymorph).[19,22,24,25] In all of these naturally occurring compounds, the Mn^{2+} cation is in an octahedral environment of S^{2-} anions. Recently, we reported some Mn^{2+}-containing thioantimonates where MnS_4 tetrahedra as well as MnN_4S_2 octahedra coexist.[4,7] In our ongoing work on the solvothermal syntheses of Mn^{2+}-containing thioantimonates by applying multidentate amines as structure directors, we found $Mn_3Sb_2S_6(C_6H_{18}N_4)$ showing a hitherto unknown structure. In this contribution, we report the solvothermal synthesis, crystal structure, and magnetic properties of this new charge-neutral inorganic−organic hybrid compound.

Experimental Section

Synthesis. The title compound was synthesized under solvothermal conditions (T = 140 °C, 7 days) by applying a mixture of 1 mmol of Sb, 1 mmol of Mn, and 2.5 mmol of S in a mixture of 2 mL of triethylenetetramine and 3 mL of H_2O. The reaction was carried out in a steel autoclave equipped with a Teflon liner. The reaction mixture was filtered and washed with H_2O, ethanol, and acetone. The product consisted of brown-reddish crystals of the title compound (yield: ca. 60% based on Sb) that are stable in air for a long period of time.

Single-Crystal X-ray Structure Determination. The data were measured using an imaging plate diffraction system (IPDS-1) from Stoe & Cie. The structure solution was performed with direct methods using *SHELXS-97*, and structure refinements were performed against F^2 using *SHELXL-97*. All non-H atoms were refined using anisotropic displacement parameters. The H atoms were positioned with idealized geometry and refined with fixed isotropic displacement parameters [U_{iso}(H) = 1.2U_{eq}(C, N)] using a riding model. Crystallographic data have been deposited with the Cambridge Crystallographic Data Centre (CCDC 751356). Copies may be obtained free of charge upon application to the Director, CCDC, 12 Union Road, Cambridge CB2 1E2, U.K. (fax int. code +(44)01223/3 36-033 and e-mail deposit@chemcrys.cam.ac.uk).

Magnetic and Heat Capacity Measurements. The direct-current magnetic susceptibilities $\chi(T)$ of a powder sample of about 70 mg were measured using a Quantum Design Magnetic Properties Measurement System (MPMS; Quantum Design, San Diego, CA). The same sample was sealed in a glass flask under ~900 mbar of ^{4}He gas to ensure thermal contact at low temperatures. The heat capacities of such samples were measured using a quasi-adiabatic heat pulse method with a home-built Nernst calorimeter similar to that described by Schnelle and Gmelin.[44] The heat capacities of the glass sample container, the sapphire platform, and a minute amount of Apiezon N vacuum grease used to thermally couple the sample to the platform were measured separately and subtracted in order to obtain the bare sample specific heat.

Table 1. Crystal Data and Results of the Structure Refinement

formula	$C_6H_{18}Mn_3N_4S_6Sb_2$
fw (g/mol)	746.92
space group	$P\bar{1}$
a (Å)	6.645(1)
b (Å)	8.667(1)
c (Å)	9.660(1)
α (deg)	90.82(2)
β (deg)	109.70(2)
γ (deg)	110.68(2)
V (Å^3)	484.4(1)
T (K)	293
Z	1
D_{calcd} (g/cm^3)	2.560
μ (mm^{-1})	5.295
λ (Å)	0.71073
R1 [$I > 2\sigma(I)$][a]	0.0363
wR2 [all data][a]	0.0930

[a] $R1 = \sum||F_o| - |F_c||/\sum|F_o|$; $wR2 = [\sum[w(F_o^2 - F_c^2)^2]/\sum[w(F_o^2)^2]]^{1/2}$.

Results and Discussion

$Mn_3Sb_2S_6(C_6H_{18}N_4)$ (**1**) crystallizes in the triclinic space group $P\bar{1}$ (Table 1). All atoms except Mn2 occupy general positions. The $Mn_4Sb_2S_6$ double-cubane unit is formed by the interconnection of one unique SbS_3 trigonal pyramid, one independent $Mn2S_6$, and one unique $Mn1S_4N_2$ octahedron. In the latter octahedron, two of the four N atoms of the amine molecule are bound to the $Mn1^{2+}$ ion. Each $Mn2S_6$ octahedron shares an edge with the SbS_3 pyramid and two edges with two symmetry-related $Mn1S_4N_2$ octahedra. The two symmetry-related $Mn1S_4N_2$ octahedra have a common edge, and each shares one edge with the SbS_3 group and one $Mn2S_6$ octahedron (Figure 1).

The $Mn2S_6$ octahedra are connected to adjacent double-cubane units by sharing one edge with a SbS_3 pyramid and one $Mn1S_4N_2$ octahedron to form one-dimensional linear rods with composition $Mn_3Sb_2S_6$ propagating along [100] (Figure 2). These rods are then joined into layers by the remaining two N atoms of the amine molecule acting in a bidentate fashion to the Mn^{2+} ion of neighboring rods. The layers extend in the (010) plane, with the shortest interlayer separation of 3.83 Å (Sb−S); i.e., the layers are well separated.

The Sb−S bond lengths as well as the S−Sb−S angles are typical for the SbS_3 trigonal pyramid and are in full agreement with literature data.[1−18] Interestingly, the Sb atoms have no next-nearest neighbor below the sum of the van der Waals radii of Sb and S (3.8 Å). It is noted that in most thioantimonate(III) compounds the Sb atom has at least one additional S atom to complete the coordination environment. The Mn1−S and Mn1−N bond lengths scatter in a narrow range (Table 2; average Mn1−S = 2.6403 Å) and are in

(14) Puls, A.; Näther, C.; Bensch, W. *Z. Anorg. Allg. Chem.* **2006**, *632*, 1239.
(15) Wang, X.; Jacobson, A. J.; Liebau, F. *J. Solid State Chem.* **1998**, *140*, 387.
(16) Cordier, G.; Schäfer, H.; Schwidetzky, C. *Rev. Chim. Miner.* **1985**, *22*, 722.
(17) Wang, X.; Liebau, F. *J. Solid State Chem.* **1994**, *111*, 385.
(18) Zhang, M.; Sheng, T. L.; Huang, X. H.; Fu, R. B.; Wang, X.; Hu, S. M.; Xiang, S. C.; Wu, X. T. *Eur. J. Inorg. Chem.* **2007**, 1606.

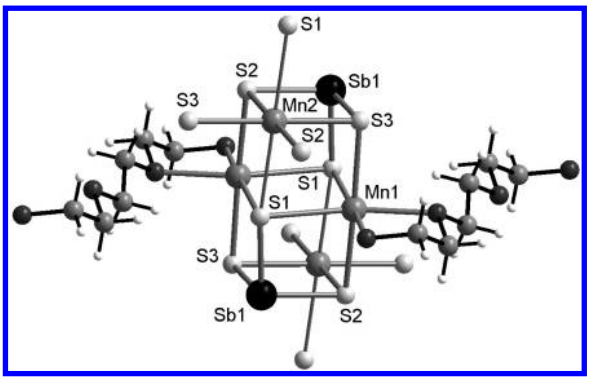

Figure 1. Double-cubane unit in $Mn_3Sb_2S_6(C_6H_{18}N_4)$ together with atom labeling. The long Mn2−S1 bonds are indicated by thinner lines. Note: C, H, and N atoms are not labeled.

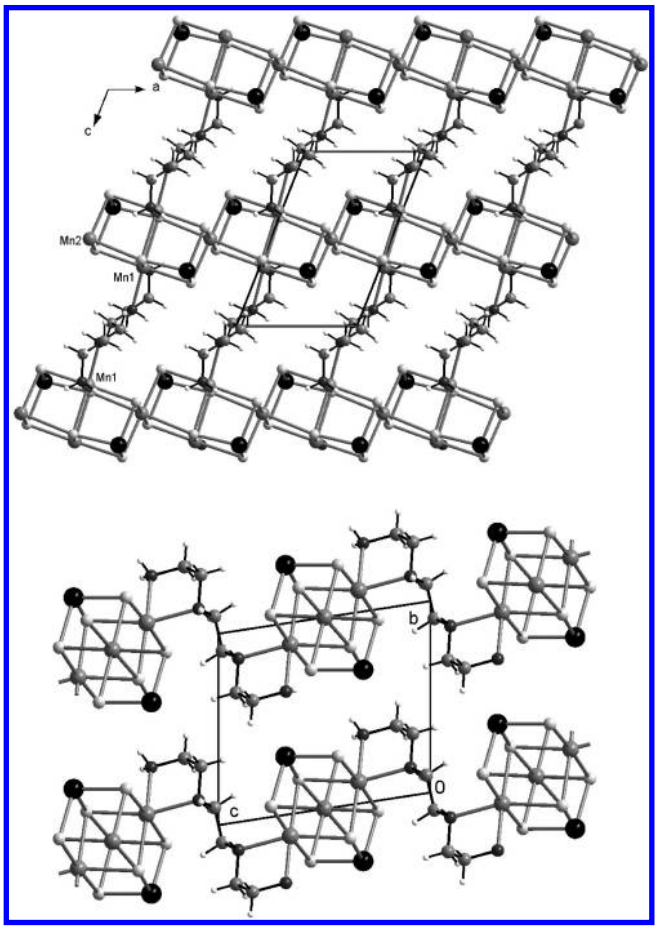

Figure 2. Two different views of the one-dimensional rods in $Mn_3Sb_2S_6$-$(C_6H_{18}N_4)$, which are interconnected into layers by the tetradentate amine molecules. Top: view onto the (010) plane. Bottom: view along [100].

agreement with the sum of the ionic radii as well as with data found in the literature.[4,7,9−14] The N/S−Mn1−S/N angles indicate a distortion of the octahedron (Table 2). The distortion is imposed as a consequence of the geometry of the organic molecule, and Mn1−N bonding is controlled by the interaction between the lone electron pair of N with the $Mn1^{2+}$ cation. The bonding situation is quite different for $Mn2S_6$ with four short Mn2−S bonds in the equatorial plane [2.5289(10)−2.5667(10) Å] and two significantly longer bond lengths to the S atoms at the apexes of the octahedron [2.8994(12) Å; Table 2]. Such long Mn−S bonds were

Table 2. Selected Interatomic Distances (Å) and Angles (deg) for the Title Compound[a]

Mn1−N2	2.279(4)	Mn2−S3	2.5289(10)
Mn1−N1	2.309(3)	Mn2−S3B	2.5289(10)
Mn1−S3A	2.6180(13)	Mn2−S2	2.5667(10)
Mn1−S1A	2.6212(11)	Mn2−S2B	2.5667(10)
Mn1−S2	2.6247(13)	Mn2−S1A	2.8994(12)
Mn1−S1	2.6973(12)	Mn2−S1C	2.8994(12)
Sb1−S3	2.4199(10)	S3−Mn2−S2	88.15(3)
Sb1−S2	2.4221(11)	S3B−Mn2−S2	91.85(3)
Sb1−S1	2.4243(12)	S3−Mn2−S2B	91.85(3)
N2−Mn1−N1	77.22(12)	S3B−Mn2−S2B	88.15(3)
N2−Mn1−S3A	89.71(11)	S3−Mn2−S1A	89.62(3)
N1−Mn1−S3A	87.83(9)	S3B−Mn2−S1A	90.38(3)
N2−Mn1−S1A	172.99(11)	S2−Mn2−S1A	85.45(3)
N1−Mn1−S1A	107.54(8)	S2B−Mn2−S1A	94.55(3)
S3A−Mn1−S1A	85.39(4)	S3−Mn2−S1C	90.38(3)
N2−Mn1−S2	94.59(11)	S3B−Mn2−S1C	89.62(3)
N1−Mn1−S2	94.19(9)	S2−Mn2−S1C	94.55(3)
S3A−Mn1−S2	175.55(4)	S2B−Mn2−S1C	85.45(3)
S1A−Mn1−S2	90.22(4)	S1A−Mn2−S1C	180.0
N2−Mn1−S1	83.46(9)	Mn1−S1−Mn2D	84.19(3)
N1−Mn1−S1	160.68(8)	Mn2−S2−Mn1	95.82(4)
S3A−Mn1−S1	92.33(4)	N1−C3	1.469(5)
S1A−Mn1−S1	91.72(4)	C1−C2	1.510(6)
S2−Mn1−S1	87.07(4)	C3−C3E	1.515(8)
N1−C1	1.477(5)	N2−C2−C1	109.2(3)
N2−C2	1.470(5)	N1−C3−C3E	110.7(4)
C3−N1−C1	110.1(3)		
N1−C1−C2	110.4(3)		

[a] Symmetry transformations used to generate equivalent atoms: A, $-x, -y, -z+1$; B, $-x+1, -y, -z+1$; C, $x+1, y, z$; D, $x-1, y, z$; E, $-x, -y, -z$.

previously observed in the series of $Mn_2(A)Sb_2S_5$ compounds,[9−14] where the values range from about 2.8 to 3.2 Å.

As mentioned in the Introduction, double-cubane units are also the main structural motif in these compounds, and from a general point of view, the title compound is a member of the series of compounds $MnSb_2S_4$,[19] $Mn_2(A)Sb_2S_5$, and $Mn_3Sb_2S_6$, i.e., $Mn_nSb_2S_{3+n}$. However, there are several pronounced differences of the double-cubane group in the title compound and those found in the structures of the $Mn_2(A)Sb_2S_5$ compounds and of $MnSb_2S_4$, which are briefly discussed here. In the $Mn_2(A)Sb_2S_5$ phases, three SbS_3 pyramids, two MnS_6 octahedra, and one MnS_4N_2 octahedron are joined to form the double-heterocubane unit; i.e., the composition of this building group is $Mn_3Sb_3S_6$, in contrast to that in the title compound. Furthermore, the Sb−S bonds within the $Mn_3Sb_3S_6$ units scatter from typical Sb−S single bonds (around 2.4 Å) to 3.4 Å, which may be treated as weak Sb−S interactions. Four such double-cubane units are then joined via common corners and edges (Figure 3, middle).

The structure of $MnSb_2S_4$ is composed of two different layers containing edge-sharing MnS_6 octahedra and SbS_5 ψ-octahedra (Sb−S bond lengths up to 3.05 Å), yielding $MnSb_3S_4$ heterocubane units. Two cubes share a common

(19) Pfitzner, A.; Kurowski, D. *Z. Kristallogr.* **2000**, *215*, 373.
(20) Moëlo, Y.; Oudin, E.; Picot, P.; Caye, R. *Bull. Mineral.* **1984**, *107*, 597.
(21) Huifang Liu, C.; Chang, L. L. Y.; Knowles, C. R. *Can. Mineral.* **1994**, *32*, 185.
(22) Léone, P.; Doussier-Brochard, C.; André, G.; Moëlo, Y. *Phys. Chem. Miner.* **2008**, *35*, 201–206.
(23) Edenharter, A.; Nowacki, W. *Z. Kristallogr.* **1974**, *140*, 87.
(24) (a) Bente, K.; Edenharter, A. *Eur. Cryst. Meeting* **1989**, *12*, 36. (b) Bente, K.; Edenharter, A. *Z. Kristallogr.* **1989**, *185*, 31.
(25) Matar, S. F.; Weihrich, R.; Kurowski, D.; Pfitzner, A.; Eyert, V. *Phys. Rev. B* **2005**, *71*, 235207-1.

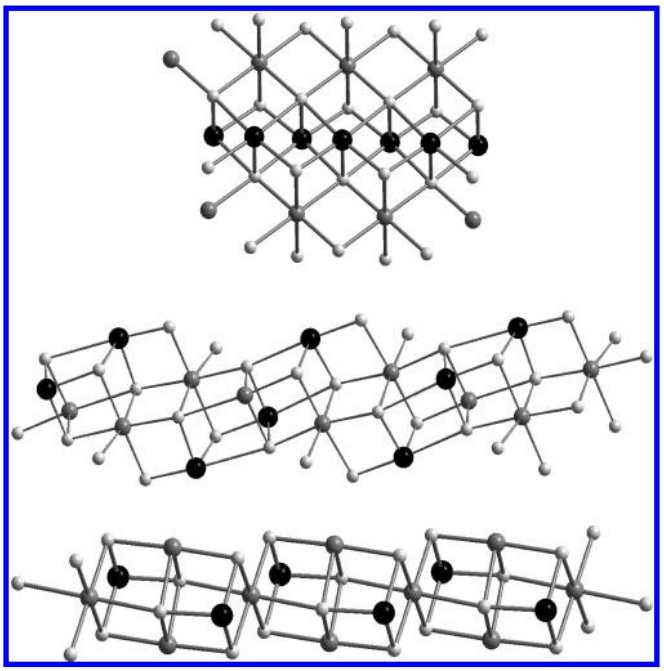

Figure 3. Cubane units in $MnSb_2S_4$ (top), $Mn_2(A)Sb_2S_5$ (middle), and the title compound (bottom). Color code: black, Sb; medium gray, Mn; light gray, S.

face to form a double-cubane group with composition $Mn_2Sb_4S_6$. The individual layers are joined to form a three-dimensional network if Sb−S distances of about 3.27 Å are considered as weak bonding interactions. The long Sb−S contacts complete the environment of one of two unique Sb atoms, yielding a distorted SbS_6 octahedron.

In all three compounds, the main building blocks are double-cubane units, but they differ in their chemical composition. With increasing Mn content in the cubanes, the dimensionality is reduced from a three-dimensional network ($Mn_2Sb_4S_4$ with $Mn_2Sb_4S_6$ double-cubane units) to a layered compound ($Mn_2(A)Sb_2S_5$ with $Mn_3Sb_3S_6$ double-cubane units) to one-dimensional rods in the title compound.

All Mn ions are in the oxidation state 2+ with a $3d^5$ electronic configuration. The topological arrangement of the Mn^{2+} cations in a diamond chain may give rise to magnetic frustration effects, as will be shown in the following. Figure 4 displays the magnetic susceptibility of **1** (per formula unit). Above ∼150 K, the susceptibility follows the Curie−Weiss law:

$$\chi_{mol} = \frac{C}{T-\theta} \qquad (1)$$

with the Curie constant C = 11.62(3) $cm^3 \cdot K/mol$ and the Weiss temperature θ = −62.0(5) K indicating predominant antiferromagnetic (afm) exchange interaction between the Mn centers. The Curie constant C is somewhat lower (∼10%) than expected for three Mn^{2+} ions with a spin-only half-filled shell configuration and an effective magnetic moment of 5.9 μ_B. The origin of this deviation is not fully clear at present. Powder X-ray diffraction patterns did not indicate any impurities. However, such may be poorly crystalline and barely visible in X-ray diffraction patterns.

Below ∼125 K, there are noticeable deviations from the Curie−Weiss behavior, with the reciprocal susceptibilities lying above the Curie−Weiss law. We ascribe these deviations

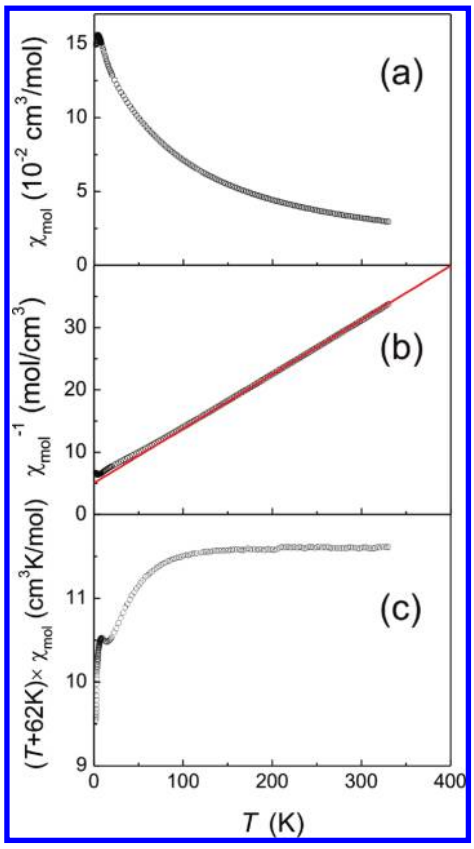

Figure 4. Temperature dependence of the low-field (0.1 T) magnetic susceptibility χ_{mol} and reciprocal magnetic susceptibility of **1** (black circles). The solid (red) line in part b results from a fit of the Curie−Weiss law to the susceptibilities above T > 150 K. (c) Plot of the temperature-dependent Curie constant defined as $(T + 62\ K)\chi_{mol}$, where 62 K is the negative Curie−Weiss temperature obtained from the fit of the reciprocal susceptibility data above 150 K (middle panel). Deviations from the Curie−Weiss law due to the gradual buildup of short-range afm correlations are clearly visible below ∼100 K.

to the buildup of increasing afm correlations due to short-range-ordering effects. These deviations are best seen in a plot of the temperature dependence of the Curie constant $C(T)$ defined as $(T - \theta)\chi_{mol}$ (Figure 4c) using θ = −62 K for the Weiss temperature as obtained from the fit of the high-temperature data (see Figure 4b).

Above 150 K, $C(T)$ attains a constant value of 11.62 $cm^3 \cdot$ K/mol, as was already obtained by the fit of the Curie−Weiss law. Below 100 K, $C(T)$ steadily decreases and passes through a shallow minimum centered at ∼15 K before it drops again below 8 K to reach a value of 9.5 $cm^3 \cdot$K/mol at lowest temperatures. The steady decrease of $C(T)$ below 8 K correlates with the broad maximum in the susceptibility and the kink at ∼2.8 K, which marks the onset of long-range afm ordering. Long-range afm ordering is also indicated by a λ-type anomaly in the heat capacity with its maximum at T_N = 2.90(5) K as displayed in Figure 5. The entropy removed in the long-range ordering amounts to ∼10% of the total magnetic entropy $3R$ ln 6 (R is the universal gas constant 8.314 J/mol·K) expected for three Mn^{2+} ions each with a spin value of $S = {}^5/_2$. This finding confirms that the essential fraction of the magnetic entropy is removed above T_N, as was already concluded from the deviations of the susceptibility from the Curie−Weiss law.

To quantitatively estimate the magnitude of the exchange constants between the Mn^{2+} centers and to model the

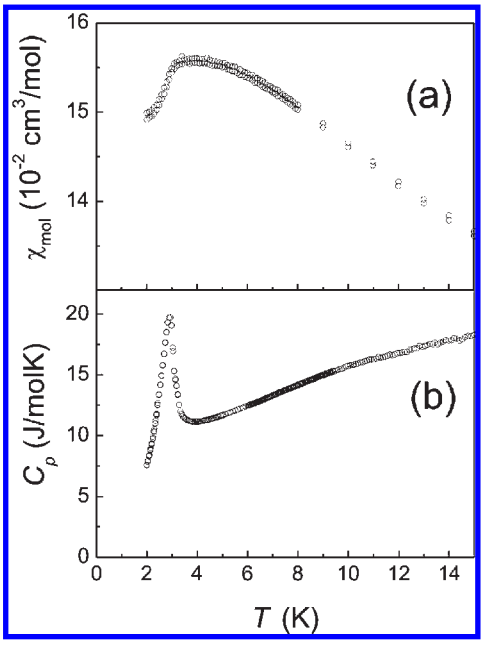

Figure 5. Low-temperature magnetic susceptibility (a) and heat capacity (b) of **1** demonstrating the onset of long-range afm ordering below T_N = 2.9 K.

magnetic behavior of the title compound, we start from the topological connectivity scheme within the polymeric $Mn_3Sb_2S_6$ chains running along the *a* axis, as shown in Figure 3, bottom. Superexchange between the Mn^{2+} centers represented by the edges is mediated by two S atoms with Mn−S−Mn bonding angles varying between ~84° and ~95°.

With this connectivity, the Mn^{2+} ions are arranged in a diamond chain with a diagonal exchange path. A similar motif is found, e.g., in the mineral azurite with Cu^{2+} ions as magnetic species. The magnetic properties of azurite currently attract special attention because of some unusual features including the aspect of magnetic frustration in a quantum system (Cu^{2+}, $3d^9$ configuration, $S = {}^1/_2$) due to the arrangement of the magnetic centers in edge-connected triangles.[26−32] Especially, the possibility that the two magnetic centers are strongly exchange-coupled across the diamonds and form a magnetic dimer includes the possibility that at low temperatures they form a nonmagnetic singlet and do not participate in the coupling along the chains anymore. We first estimate the average magnitude of the superexchange $\bar{J}$ by using the simple relation (2), which connects $\bar{J}$ with the Weiss temperature θ according to[33]

$$\theta = -\frac{2}{3}S(S+1)\sum_{ij} J_{ij} \approx -\frac{2}{3}S(S+1)\bar{J}z_{\text{eff}} \qquad (2)$$

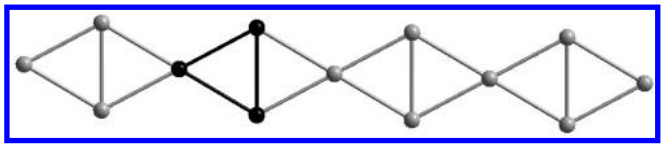

Figure 6. Connectivity in the polymeric $Mn_3Sb_2S_6$ chains showing the diamond-chain arrangement of the Mn^{2+} ions. A single repetition unit, a $[S = {}^5/_2]_3$ triangle, is highlighted in black. Each edge represents a superexchange path resulting from two bridging S atoms with Mn−S−Mn bonding angles close to 90°.

J_{ij} are the exchange constants between neighboring Mn^{2+} ions coupled by a Heisenberg Hamiltonian using the convention

$$H = -2\sum_{ij} J_{ij}\vec{S_i}\vec{S_j} \qquad (3)$$

In eq 2, we have simplified the summation over all possible exchange paths such that we consider z_{eff} nearest-neighbor interactions only and that we assume as an approximation that J_{ij} does not vary very much and can be well approximated by the average value $\bar{J}$. Using eq 2 with θ = −62 K and z_{eff} = 3, we obtain

$$\bar{J} = -3.5K \qquad (4)$$

This approximation is obtained by assuming an effective coupling, and it neglects any structure in the Mn structural arrangement. In order to model the diamond chain, we proceeded in the following way: Each edge connecting the Mn^{2+} ions represents a superexchange path (Figure 6) due to coupling of the Mn^{2+} centers via S bridges. If antiferromagnetically coupled, such resulting Mn triangles (Figure 6) will give rise to substantial competing interaction and magnetic frustration. A clear indication that magnetic frustration in the $Mn_3Sb_2S_6$ chain plays an essential role is immediately provided by the so-called frustration index *f* defined as the ratio of the Curie−Weiss temperature θ and the Néel temperature T_N,[34] which for $Mn_3Sb_2S_6(C_6H_{18}N_4)$ amounts to

$$f = |\theta|/T_N = 62\text{ K}/2.9\text{ K} \approx 21$$

In order to model the magnetic susceptibility and to extract exchange constants, we therefore have to take into account the one-dimensional character of the $Mn_3Sb_2S_6$ chains as well as the triangular arrangement and the aspect of frustration within the chains. To the best of our knowledge, theoretical calculations for such a diamond chain with $S = {}^5/_2$ magnetic moments are not available in the literature. Susceptibility calculations for similar arrangements of the magnetic ions but with magnetic moments in the extreme quantum limit with a spin $S = {}^1/_2$ have recently become available and been used to fit the magnetic susceptibility, e.g., of azurite, $Cu_3(OH)_2(CO_3)_2$.[27,28,35]

In the following, we describe a procedure that allows one to model successfully the magnetic susceptibility over the whole temperature range down to ~4 K. In this model, we decompose the $Mn_3Sb_2S_3$ chains into trimer units. For simplicity, we also assume a symmetric case such that the Mn^{2+} cations

(26) Kang, J.; Lee, C.; Kremer, R. K.; Whangbo, M.-H., submitted for publication.
(27) Kikuchi, H.; Fujii, Y.; Chiba, M.; Mitsudo, S.; Idehara, T. *Physica B* **2003**, *329−333*, 967–968.
(28) Kikuchi, H.; Fujii, Y.; Chiba, M.; Mitsudo, S.; Idehara, T.; Tonegawa, T.; Okamoto, K.; Sakai, T.; Kuwai, T.; Ohta, H. *Phys. Rev. Lett.* **2005**, *94*, 227201.
(29) Bo, G.; Su, G. *Phys. Rev. Lett.* **2006**, *97*, 089701.
(30) Kikuchi, H.; Fujii, Y.; Chiba, M.; Mitsudo, S.; Idehara, T.; Tonegawa, T.; Okamoto, K.; Sakai, T.; Kuwai, T.; Ohta, H. *Phys. Rev. Lett.* **2006**, *97*, 089702.
(31) Li, Y.-C. *J. Appl. Phys.* **2007**, *102*, 113907.
(32) Mikeska, H.-J.; Luckmann, C. *Phys. Rev. B* **2008**, *77*, 054405.
(33) Nolting, W. *Quantentheorie des Magnetismus*; Teubner: Stuttgart, Germany, 1986; Vol. *2*.
(34) Schiffer, P.; Ramirez, A. P. *Comments Condens. Matter Phys.* **1996**, *10*, 21.
(35) Honecker, A.; Läuchli, A. *Phys. Rev. B* **2001**, *63*, 174407.

in the trimers are all coupled by a Heisenberg exchange J_{trimer} according to

$$H = -2J_{trimer}(\vec{S_1}\vec{S_2} + \vec{S_1}\vec{S_3} + \vec{S_2}\vec{S_3}) \quad (5)$$

The magnetic properties of the trimers were treated in the 1950s in the investigation of polynuclear systems by Kambe containing Fe^{3+} and Cr^{3+} with $S = {}^5/_2$ and ${}^3/_2$, respectively.[36] By using Van Vleck's equation, we calculate a temperature-dependent effective magnetic moment $\mu^2_{eff}(T)$ for the spin trimers according to[37]

$$\mu_{eff}{}^2(T) = g^2 \frac{\sum_{S_T} S_T(S_T+1)(2S_T+1)\exp[-E_{spin}(S_T)/k_BT]}{\sum_{S_T}(2S_T+1)\exp[-E_{spin}(S_T)/k_BT]} \quad (6)$$

where g is the g factor, which for Mn^{2+} with a spin-only magnetism can be assumed to be very close to 2, S_T is the total spin of a magnetic trimer, which can vary between ${}^5/_2$ and ${}^{15}/_2$, and the summation is carried out over all possible spin configurations. We subsequently define a temperature-dependent effective spin $S_{eff}(T)$ for such a trimer according to

$$g^2 S_{eff}(T)\,[S_{eff}(T)+1] = \mu_{eff}{}^2(T)/3 \quad (7)$$

Such effective spins are then coupled to a chain for which the magnetic susceptibility is calculated by employing the Bonner equation for a classical Heisenberg chain with nearest-neighbor coupling. The susceptibility of a Heisenberg chain with large spins $S \rightarrow \infty$ is given by[38]

$$\chi_{CH}(T) = \frac{Ng^2\mu_{Bohr}{}^2 S(S+1)}{3k_BT}\frac{1+U(K)}{1-U(K)} \quad (8)$$

where

$$U(K) = \coth(K) - \frac{1}{K} \quad (9)$$

and

$$K = \frac{2J_{chain}S(S+1)}{k_BT} \quad (10)$$

For the spin S, we now introduce the effective spin $S_{eff}(T)$ of the trimer calculated according to eq 7. This scheme of treating a subunit exactly and coupling an effective spin to a chain bears similarities to the Oguchi method and has, e.g., been used to model the magnetic susceptibility of the rare-earth chain compound Gd_2Cl_3.[39−41]

This minimal model neglects any deviation from a symmetric magnetically highly frustrated trimer by assuming equal exchange coupling along the edges. It provides a very good description of the magnetic susceptibility of **1** as shown in Figure 7.

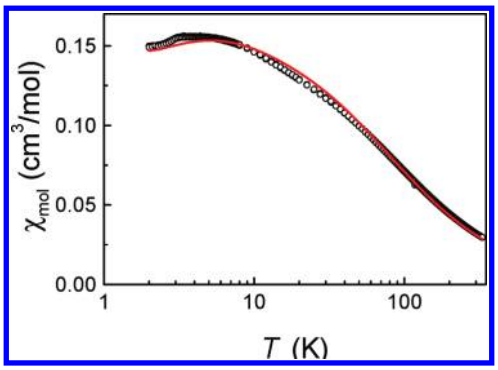

Figure 7. Magnetic susceptibility of **1** (○) fitted to the theoretical heat capacity model of spin trimers forming the spin entities of a Heisenberg chain as described in the text. The effective afm exchange coupling parameters extracted from the fit are $J_{trimer} = -2.2(1)$ K and $J_{chain} = -1.9(1)$ K (for further details, see the text).

As fitting parameters, we varied the trimer exchange parameter J_{trimer}, the exchange J_{chain} along the chain, and a scaling factor to take care of the reduction of the susceptibility described above.

This scaling factor is found to be close to 2.5, consistent with the reduction of the high-temperature effective magnetic moment by 10% possibly due to nonmagnetic impurities as discussed above. The effective afm exchange coupling parameters for the spin trimer and the coupling along the chain are both afm, indicating substantial magnetic frustration within the $Mn_3Sb_2S_6$ chains, as was already indicated by the large frustration ratio close to 20 (see above). The fitted exchange parameters are very similar and amount to

$$J_{trimer} = -2.2(1)\ \text{K} \quad \text{and} \quad J_{chain} = -1.9(1)\ \text{K}$$

The magnetic susceptibility gives a strong indication that the magnetic properties of the $Mn_3Sb_2S_6$ chains have a strong one-dimensional character. The magnetic contributions to the heat capacity of **1** should therefore extend to temperatures significantly above the Néel temperature.

A closer inspection of the heat capacity above the Néel temperature revealed deviations from a T^3 power law, as may be expected for the Debye-like behavior of the lattice contributions to the heat capacity. These deviations may indicate significant magnetic contributions to the heat capacity far above the Néel temperature, as may be expected from short-range ordering contributions of a one-dimensional magnetic system.[41] A quantitative estimation of the magnetic contributions can be useful in supporting the conclusions made from the fitting of the magnetic susceptibility data. In order to separate lattice and magnetic contributions, we proceeded in the following way:

(1) We assume that the lattice contributions sufficiently far above the Néel temperature ($T > 50$ K) can be approximated by a power law in T, with contributions essentially from odd powers in T. To consider also magnetic contributions at high temperatures, i.e., a contribution $\propto T^{-2}$, we add a Padé approximant to the heat capacity of a linear chain with spin S according to Rushbrooke and Wood[42]

$$\frac{C_{mag}}{R} = \frac{4S^2(S+1)^2}{3t^2}\left(1 + \sum_n \frac{c_i}{t^n}\right) \quad (11)$$

(36) Kambe, K. *J. Phys. Soc. Jpn.* **1950**, *5*, 48.
(37) Van Vleck, J. H. *The Theory of Electric and Magnetic Susceptibilities*; Oxford University Press: Oxford, U.K., 1932.
(38) Bonner, J. C.; Fisher, M. E. *Phys. Rev.* **1964**, *135*, A640.
(39) Kremer, R. K. Ph.D. Thesis, Technische Universität, Darmstadt, Germany, **1985**.
(40) Majilis, N. *The Quantum Theory of Magnetism*, 2nd ed.; World Scientific: London, 2007.
(41) de Jongh, L. J.; Miedema, A. R. *Adv. Phys.* **1974**, *23*, 1.
(42) Rushbrooke, G. S.; Wood, P. J. *Mol. Phys.* **1958**, *1*, 257.

where the reduced temperature and the Padé coefficients are given by $t = T/J$ and c_i, respectively. The Padé coefficients c_i were determined by fitting eq 11 to the heat capacity data of a $S = {}^5/_2$ afm Heisenberg chain, as obtained by Blöte from numerical diagonalization of the Hamiltonian given by eq 3.[43]

For the Padé coefficients up to seventh order, we obtained

$$c_1 = -1.30935(0.15035)$$

$$c_2 = 94.17052(4.76879)$$

$$c_3 = -299.48126(55.38188)$$

$$c_4 = 3375.60378(300.2205)$$

$$c_5 = -9554.17132(793.57258)$$

$$c_6 = 14985.16288(980.22763)$$

$$c_7 = -8677.43907(448.40058)$$

Figure 8a shows the heat capacity of **1** together with the estimated lattice contribution. The difference represents the magnetic contribution to the heat capacity, which is displayed in Figure 8b, together with theoretical heat capacities for a Heisenberg chain and a spin diamond. The magnetic heat capacity shows a typical Schottky-like anomaly attaining its maximum value of about 20 J/mol·K at 22(1) K. A comparison with the heat capacities calculated for the $S = {}^5/_2$ afm Heisenberg chain with an exchange constant $J = -4$ K or the heat capacity of a spin tetramer (diamond) with an exchange of -3 K along the edges compares rather well with the difference data, confirming our conclusions drawn from the magnetic susceptibility that the magnetic properties of **1** are essentially determined by the one-dimensional character of the $Mn_3Sb_2S_6$ chains. The magnetic susceptibility shows a broad feature also centered around ≈25 K, which evidences significant magnetic frustration due to the arrangement of the Mn^{2+} ions in a triangular configuration.

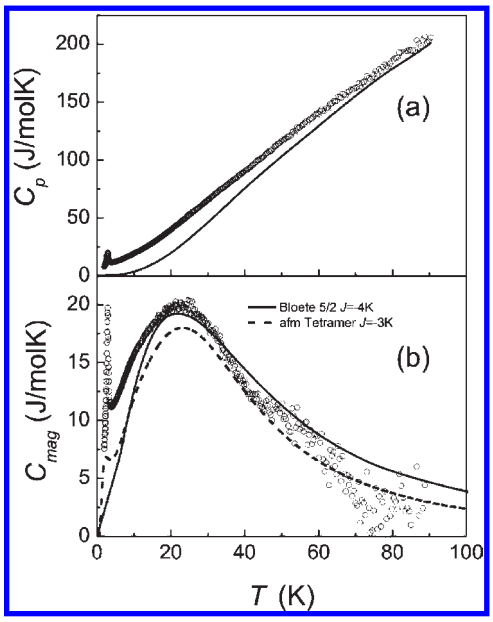

Figure 8. (a) Heat capacity of **1** (○) and estimated lattice contribution to the heat capacity (solid line; for details, see the text). (b) (○) Difference of the total heat capacity and the estimated lattice heat capacity, i.e., magnetic contribution to the heat capacity (C_{mag}) of **1**. The solid line represents the heat capacity of a $S = {}^5/_2$ afm Heisenberg chain with an exchange constant of $J \sim -4$ K (according to Blöte) and the heat capacity of a symmetric spin tetramer (a diamond without diagonal coupling) with afm exchange of -3 K (dashed line).

In summary, the magnetic susceptibility and the magnetic contributions to the heat capacity are consistent with the assumption of a one-dimensional chain model containing effective spin entities composed of frustrated spin triangles. The typical afm exchange parameters range within a regime of -2.2 to -4 K, as evidenced by the analysis of the magnetic heat capacity and the magnetic susceptibility.

(43) Blöte, H. W. J. *Physica* **1974**, *78*, 302.
(44) Schnelle, W.; Gmelin, E. *Thermochim. Acta* **2002**, *391*, 41.